

Chapter 1

The magnetic nature of intrinsic and irradiation-induced defects in carbon systems

**Petri O. Lehtinen¹, Arkady V. Krasheninnikov^{1,2}, Adam S. Foster¹
and Risto M. Nieminen¹**

¹Laboratory of Physics, Helsinki University of Technology, P.O. Box 1100,
02015, Finland

²Accelerator Laboratory, University of Helsinki, P.O.Box 43, Helsinki 00014,
Finland

1.1 Introduction

Observations of magnetism in various carbon systems [1, 2, 3, 4] have stimulated much experimental and theoretical research work (Ref. [5] and references therein) on the magnetic properties of all-carbon systems. The driving force behind these studies was not only to create technologically-important, light, non-metallic magnets with a Curie point well above room temperature, but also to understand a fundamental problem: the origin of magnetism in a system which traditionally has been thought to show diamagnetic behavior only.

The question which immediately springs to ones mind is whether magnetism is an intrinsic property of carbon systems or is due to the presence of magnetic impurities (e.g., Fe). The debate was initiated from the appearance of the two classic papers: in 2000 Kopelevich and coworkers published a paper [1] with an editor's note of the controversial nature of the result. In that work, the authors identified ferromagnetic and superconducting-like magnetization hysteresis loops in highly oriented pyrolytic graphite samples below and above room temperature. The conclusion was that magnetic impurities were extremely unlikely. In 2001 Makarova and coworkers [2] reported a discovery

of strong magnetic signals in rhombohedral C60. Their intention was to search for superconductivity in polymerized C60; however, it appeared that their high-pressure, high-temperature polymerization process resulted in a magnetically ordered state. The material exhibited features typical of ferromagnets: saturation magnetization, large hysteresis and attachment to a magnet at room temperature. A careful analysis carried out in the original [2] and follow-up works [3, 6, 7] showed that one can exclude magnetic impurities as the origin of ferromagnetism.

If magnetism is indeed the intrinsic property of carbon systems, then the most important questions to be answered are as follow:

1. *What is the atomic structure of the magnetic phase and what is the local bonding geometry which gives rise to the net magnetic moment?*

The presence of local magnetic moments can explain only the paramagnetic behavior but not ferromagnetism. Thus, the second question is:

2. *How is the macroscopic ferromagnetic state formed and what is the mechanism of long-range order formation?*

Because ferromagnetic signals have been detected in various carbon systems such as graphite [1, 4, 6] polymerized fullerenes [2], and carbon foam [3], it is highly important to understand:

3. *Is the mechanism of magnetic state formation common for all the carbon systems or is it different for different allotropes?*

Finally, if magnetism is not the intrinsic property of all-carbon systems and it does not originate from magnetic impurities, then another question rises:

4. *Can magnetism result from impurity atoms which are non-magnetic by themselves, but due to unusual chemical environment, e.g., due to bonding to defects in graphitic network, give rise to local magnetic moments?*

As for the first problem, a number of factors are nowadays thought to possibly give rise to appearance of localized spins and the development of the magnetic state in all-carbon systems: defects in the atomic network such as under-coordinated atoms [8, 9, 10, 11, 12, 13], itinerant ferromagnetism [14, 15] and negatively-curved sp^2 -bonded nano-regions in the carbon structures [3, 16] (see also chapter [Rode]). Among these factors the defect-mediated mechanism appears to be the most general one because negatively-curved regions can hardly be found in graphite, and as for the second scenario, although itinerant mechanisms resulting from strong electron-electron interactions and the effective dimensionality of the electron system can give rise to magnetism, direct experimental evidence supporting such a mechanism is still lacking.

The defect-mediated mechanism has been addressed in a considerable number of works [8, 9, 10, 11, 12, 13]. Although the details can be different for different carbon systems (polymeric fullerenes, graphite, nanotubes), the common feature is the presence of under-coordinated atoms, e.g., vacancies [11, 17] (see also chapter [Andriotis]), atoms on the edges of graphitic nano-fragments with dangling bonds either passivated with hydrogen atoms [12, 13, 18] (see also chapter [Wakabayashi,Kusakabe]) or free [10, 13]. Structural defects, in general,

give rise to localized electronic states, a local magnetic moment, flat bands associated with defects and thus to an increase in the density of states at the Fermi level, and eventually to the development of magnetic ordering. However, even if this conjecture is correct, it is not clear at all whether such defects are actually present or if their concentration is high enough to provide the magnetic moment observed in the experiments.

At the same time, it is well known that irradiation of carbon systems with energetic electrons and ions should give rise to defects, and their number can be controlled by choosing the right irradiation dose, particle energy and irradiation temperature. Thus, if irradiation of the originally non-magnetic carbon samples gave rise to magnetism, this could be strong evidence for the defect scenario.

Graphite samples were recently irradiated with 1.5 MeV He and 2.25 MeV H ions [19, 20] (see also chapter [Esquinazi]). It was found that proton bombardment produced a strong magnetic signal, while bombardment with helium ions produced a signal which was only slightly larger than background.

To explain the irradiation-induced magnetism and shed light on the role of defects in all-carbon magnetism, the atomic structure and magnetic moment of various defects were recently calculated [21, 22, 23, 24] at the atomistic level within the framework of Density Functional Theory (DFT).

In this Chapter, we give a summary of the most important theoretical results obtained in Refs. [21, 22, 23, 24] and try to answer questions (*i*) and partly (*iv*) listed above. We address the behavior of various point defects—vacancies, interstitials and more complicated aggregations, both intrinsic, and those which can appear in carbon nanotubes and graphite under irradiation. We briefly describe not only magnetic, but also structural and other characteristics of the defects, such as formation energies and diffusivity. We show that under certain conditions the defects can indeed give rise to magnetism. We further consider defects which can appear under proton irradiation and demonstrate that even a small amount of hydrogen in carbon samples might be very important for the formation of the magnetic state.

1.1.1 Intrinsic defects

There are several classes of intrinsic defects, such as grain boundaries and dislocations [25], but here we focus on the more universal point defects. There are two main types of intrinsic point defects: vacancies and interstitials. A vacancy is one missing atom and an interstitial is an extra atom in the crystal. It is obvious that if we displace a carbon atom from its original position in the lattice of a real crystal, we create not only a vacancy, but also an interstitial. The vacancy-interstitial pair is known as a Frenkel pair. These defects are usually the cause for the observed conductivity of ionic crystals and they have a significant effect on the optical properties (specially on the color). They are present in the thermal equilibrium which makes them intrinsic of nature [25].

Besides vacancies and interstitials, there are other types of simple defects, such as Stone-Wales defects (two heptagons and two pentagons), formed by rotating a carbon-carbon bond by 90 degrees [26]. The barrier for such defect formation is lower than that for Frenkel pairs, especially if an extra carbon atom which works as a catalyst is nearby [27]. However, this defect is non-magnetic, so we do not consider it further.

1.1.2 Irradiation-induced defects in graphitic structures

When an energetic particle such as an electron or ion hits the material, different mechanisms of damage creation can work. Depending on the target material and the incident particle characteristics, the main mechanism can be the direct kinetic energy transfer to target atoms (nuclear stopping) or the transfer of the projectile energy to the target electrons via electronic excitations, ionization, *etc.* (electronic stopping) [28]. For light ions (such as H, He), electronic stopping is more important. For heavy ions nuclear stopping dominates at low energies, while electronic effects govern energy loss at high energies with the crossover point being dependent on the ion mass [28]. The damage production is further dependent on the electronic structure of the target (metal/insulator). As *sp*² carbon systems are either metals or narrow-band semiconductors, electronic excitations and ionization effects seem to be less important [29] in graphitic systems than in diamond due to a high electrical conductivity of the *sp*² carbon network.

However, whatever the main channel of the energy transfer is, irradiation gives rise to the formation of Frenkel pairs. In addition to single point defects, defect aggregations (vacancy and interstitial clusters) can appear either directly due to impact of the energetic particle or due to defect migration and annealing. A review of irradiation defect production and annealing in graphitic systems can be found in Refs. [29, 30, 31].

Note that due to the open structure of carbon nanotubes (CNT) and a low density of the nanotube samples, the damage formation in carbon nanotubes is quite different from that observed in most other solids. Due to the open space in the CNT samples, even recoils which have received energy only slightly above the threshold energy can be displaced quite far, which is in contrast to many other types of materials.

There are also differences in defect annealing. In semiconductors such as Si a vast majority of all Frenkel pairs produced are known to recombine below room temperature [32]. In dense metals, nearly all the interstitials and vacancies produced during the ballistic phase of the cascade recombine with each other after only a few picoseconds, regardless of the sample temperature [33]. Defects in CNTs can also anneal, but it happens at elevated temperatures [29], and the annealing mechanisms are somewhat different from those in metals [31]. In particular, single and multiple vacancies can disappear by saturating dangling bonds [34, 35] and by forming non-hexagonal rings. This mechanism works in graphite as well, but in CNTs it is more important as finite curvature of graphene sheets decreases transformation-induced strain in the atomic network.

1.2 Methodology

Most of the calculations described here are made using the periodic plane wave VASP code [36, 37], implementing the spin-polarized density functional theory (DFT) and the generalized gradient approximation (GGA) of Perdew *et al* [38]. DFT can also be implemented for finite systems, using other basis sets than plane waves (e.g. gaussians), but in standard DFT simulations this recipe is the most accurate, as errors are much more controllable. Also, since we are dealing with either an infinite graphite surface or CNT, the periodicity implied by plane

waves is not a hindrance.

In any case, rather than going into technical details, it is perhaps more useful to give some consideration to the general issues important in modelling defects with this method.

1.2.1 Periodic model

The periodic model is based on a definition of a unit cell (or more generally - supercell), which can be periodically translated to build an infinite system. There are no limitations, in principle, on the size and shape of the unit cell providing that the host lattice is defined unambiguously. The periodicity imposed on the atomic structure also applies to the electronic structure: the charge density is the same in every supercell and is matched at the boundary between two neighboring supercells. In the case of ideal crystals this approach is technically exact. For surfaces, a very good model can be achieved by making the vacuum gap in the z-direction between images of the surface large enough to avoid interactions - this is known as the “slab” model. To calculate the properties of an individual point defect using the periodic model, a supercell is defined which comprises the defect and its immediate environment. The defect in each supercell interacts with an infinite number of similar defects (called images) in all other supercells.

An obvious feature of the periodic model, which can be both to its advantage and drawback, is that ”defects” are periodically translated and interact between themselves. It can be an advantage if one is interested, for example, in periodic adsorption of molecules at the surface and would like to vary their concentration. It is a drawback if one is interested in the properties of an individual defect in different charge states. In particular, if the defect is charged with respect to the host lattice, the electrostatic interaction of such defects is divergent. Yet another downside of the periodic model is that the defect-induced distortion of the host lattice can only be taken into account within the supercell. This may lead to inaccurate results if these distortions propagate further than cell boundaries, but can be checked by increasing the supercell size. Several recent developments in computational techniques using the periodic model have led to an improvement of their treatment of defects:

- A neutralizing background is introduced to calculate defects which are charged with respect to the host lattice. With this background the supercell becomes neutral and the electrostatic summation can be carried out.
- The total energy obtained from the periodic model calculation includes the interaction of the defect with its images. Providing that the interaction between the images is well reproduced by low-order multipoles, it is possible to extract the energy associated with an isolated defect as suggested by Makov and Payne for cubic supercells [39] and generalized for arbitrary supercells by Kantorovich [40].

Finally, studying excited states in the periodic model represents a difficult problem. On one hand, excited states are often much more delocalized than the system ground state and hence require much bigger cells for reliable predictions. On the other hand, computational techniques for calculating excited

states are developed in the periodic model to a lesser extent than those available for molecules and in a cluster model.

To summarise, the periodic model is ideal if one is interested in the ground state properties of neutral defects, which weakly perturb the surrounding lattice.

1.2.2 Density functional approach

The Density Functional Approach is based on two theorems by Kohenberg and Kohn which state that: i) the ground state energy of a non-degenerate electronic state is a unique functional (density functional) of its density, $E[\rho]$. ii) the energy can be obtained by variation of the universal density functional with respect to the charge density. This implies that calculation of the wave-function of the many-electron system is not required in order to find the total energy, only the charge density is required. However, the exact density functional is not known and some approximate functionals are used instead.

The functional E can be divided into terms which describe the kinetic energy of electrons, their interaction with the external potential, their electrostatic interaction with each other and, finally, the term which accounts for the exchange and electron correlation, E_{xc} . It is this latter term that is not known and needs to be approximated. A widely used Local Density Approximation (LDA) assumes that the exchange-correlation energy E_{xc} for each element $\rho(r)dr$ is the same as for the uniform electron gas of density $\rho = \rho(r)$. This is very convenient because the uniform electron gas remains the only system for which E_{xc} can be calculated exactly.

Although the LDA is clearly a very strong approximation, it has proved to be very successful in predicting the geometric structure and electronic properties of many materials. Its obvious deficiency is that it neglects the effect of fast-changing electron density on the exchange-correlation energy, E_{xc} . This results in systematically underestimated equilibrium inter-atomic distances predicted by this method. To account for this effect functionals were developed which also include the dependence on the gradient of density. This scheme is known as the Generalised Gradient Approximation (GGA).

Some of the disadvantages of DFT relevant to further discussion include systematically under-estimated single particle band gaps and an overall tendency to delocalise the electron density. This is particularly relevant to the calculations of defects in insulators because too narrow band gaps make it difficult or impossible to describe shallow defect states. Similarly, the tendency to delocalize the electron density can, and often does, lead to qualitatively wrong conclusions regarding defect electronic structure (see, for example, discussion in refs. [41, 42, 43]). Addressing this issue remains a strong focus of methods research in materials science, and several possibilities exist. The so-called GW perturbation theory [44] offers highly accurate gaps in semiconductors, both quantum Monte Carlo (QMC) [45] and time-dependent DFT [46] give improved gaps at the cost of greatly increased computational resources.

Some of the problems discussed above can also be eliminated if one combines the advantages of DFT and exact exchange from Hartree-Fock in the so-called hybrid density functional approach. Perhaps the most widely used hybrid functional is due to Becke [47] and is called B3LYP [17]. It has demonstrated great improvements in many systems including MgO, alumina and TiO₂ [48]. In this functional, the correlation term in the E_{xc} is the one suggested by Lee, Yang

and Parr [49] (hence LYP), and the exchange term is the sum of three contributions including the Hartree-Fock exchange weighed with some parameters (this is what the number 3 in B3LYP stands for). The parameters were fitted to reproduce the ionization potentials, electron affinities of atoms and dissociation energies of a large number of molecules. An accumulated experience demonstrates that the B3LYP parameterization is good at reproducing both atomic and electronic properties of many ionic materials, and is widely used in both periodic and cluster calculations. However, the fact that B3LYP includes to some extent the HF exchange makes it a non-local functional and it is therefore implemented only in computer codes using localized basis sets.

One problem which cannot be fully corrected with any standard functionals discussed here, is the incorrect representation of the van der Waals interaction in DFT. In practice, LDA will give reasonable agreement with experiment for the interlayer distance in graphite, but this is due to chance rather than evidence of a good physical representation. Detailed analysis of the decay of the interaction shows that it does not reproduce the true van der Waals, and accurately including this requires more advanced methods [50].

Plane-wave basis set

The basis set controls the accuracy of calculations for a given method and its boundary conditions. The plane wave (PW) basis can only be used in conjunction with periodic boundary conditions. It is very effective in practical calculations because: i) it is an orthogonal basis, and ii) a product of two plane-waves is also a plane-wave and their derivatives are products in k-space. Due to these PW properties and very effective computational methods exploiting the periodicity of the system, the number of atoms that can be included in a supercell is generally a few times larger than the number of atoms in cluster calculations for comparable accuracy. The PW basis is independent of atomic positions and spans the whole supercell uniformly. For the given size of the supercell, it can be systematically saturated by increasing a single parameter - the cutoff energy, E_c . The value of E_c is determined by the highest density curvature. This implies that the description of the core electrons requires inaccessibly large values of E_c . To overcome this problem the PW basis is used together with pseudopotentials representing atomic cores (see, for example, [51, 52]), or with the more elegant projector augmented-wave method (PAW) [53, 54]. On the other hand, regions of small and weakly changing electron density are described with excessive accuracy. This substantially increases the computational expense in calculations where there is a lot of free space, such as cage systems or surfaces.

Tight-binding method

DFT-based and other first-principle *ab initio* methods have a high computational cost, which makes the use of such methods in practice impossible for tackling some problems, e.g., formation of defects under irradiation or direct dynamical simulations of defect diffusion.

To address such issues, a number of computationally cheaper methods have been developed, such as empirical potential and tight-binding simulation techniques.

The main difference between these two methods is that the empirical potential energy is described by an analytical function of atom coordinates usually fitted to experimental data, whereas in the tight-binding method the energy is calculated by solving the Schrödinger equation for electrons in the field of atom cores, although the exact many-body Hamiltonian operator is replaced with a parameterized Hamiltonian matrix. The basis set usually is atomic-like so that it has the same symmetry properties as the atomic orbitals.

The drawback of the empirical approach is its low accuracy and transferability (the ability to describe systems different from those used for fitting the parameters). At the same time, although first-principles methods generally provide the best overall accuracy, the tight-binding approach is a reasonable compromise between the computational efficiency and the reliability of the model used.

Therefore, in addition to the PW DFT method, in our simulations we used a non-orthogonal self consistent charge tight-binding method [55, 56] in which the parameters of the Hamiltonian were derived from *ab initio* calculations (a second-order expansion of the Kohn-Sham total energy in DFT with respect to charge density fluctuations). Thus, no empirical parameter is present in the method and despite the approximations made this method retains the quantum-mechanical nature of bonding in materials, ensuring that the angular nature of the bonding is correctly described in far-from-equilibrium structures. Due to parameter fitting to the density functional results, this method, unlike other tight-binding schemes (where the parameters are chosen to describe equilibrium structures) describes the interaction of atoms even at small interatomic separations, i.e., upon energetic collisions. This approach has been found to work well in modeling various systems [57] and the results are in agreement with those obtained by the first-principles methods [22].

1.3 Magnetic properties of the Frenkel pair in carbon systems

As discussed in the introduction, one of the most probable intrinsic defect present in carbon samples is the Frenkel pair. Since recombination of proximate Frenkel partners is very probable, in this section we consider the properties of isolated adatoms and vacancies in carbon systems - specifically a graphene sheet and various nanotubes.

The abundance of open space in nanotubes suggests that the interstitial atom can also be treated as an *adatom* adsorbed onto the nanotube surface [58, 35]. This is particularly the case for isolated single-walled nanotubes (SWNT) and interstitials in the inner cores of the tubes. However, the nature of the vacancies and interstitials in graphite and multiwalled nanotubes (MWNT) is complicated by the presence of nearby layers. If we consider graphite as an example, it is clear that the properties of vacancies and interstitials may be affected by the presence of the second layer. However, as discussed in the previous section, any treatment of interlayer processes with DFT ignores the fact that the van der Waals interaction between layers is incorrectly represented. Hence, it is probably better, and still qualitatively correct, to consider only a single graphene sheet as a good model of graphite.

1.3.1 Adatom on graphene

The first *ab initio* calculations concerning the properties of an adatom on a single sheet of graphite (graphene) were performed by Mattila and coworkers [59] in the middle of 1990's. Using a 50-atom size sheet and LDA they concluded that the ground-state of an adatom is a bridge-like structure (the starting and endpoints of the migration paths in Fig. 1.2).

The development of computing techniques and computers alongside the renewed interest on the carbon materials made it tempting to recalculate the ground-state properties of the carbon atom on a sheet of graphite. Using GGA, we found a similar ground state bridge structure [21]. The equilibrium position of the adatom was found to be in a bridge-like structure, between two surface carbon atoms. This geometry is similar to previous local density approximation (LDA) calculations [59, 60, 61] on a similar surface. The perpendicular distance of the adatom to the graphite surface is 1.87 Å. The adsorption energy of the defect was found by moving the adatom far from the surface until total energy convergence, and once again fully relaxing the surface to find the difference in energy. Note that the ground state for the isolated carbon atom is a triplet state, and we use this as a reference for our adsorption energies (to compare with adsorption energies referenced to the singlet state, 1.26 eV should be added to the values). The adsorption energy was found to be 1.40 eV (1.37 eV for the 72 atom slab). This is similar to the 1.2 eV [60] and 1.78 eV [61] found in finite cluster LDA studies, but smaller, even when comparing with the singlet reference adsorption energy of 2.66 eV, than the 3.30 eV found in previous periodic LDA works [59]. We also considered adsorption of an adatom directly on top of a surface carbon and found this to be over 1.0 eV higher in energy than the bridge structure

In contrast to previous studies, we used fully spin-polarized DFT in our calculations and found that the ground state for the adsorbed adatom has a magnetic moment of $0.45 \mu_B$. Earlier finite cluster LDA calculations [60] also found a magnetic ground state for an adatom adsorbed on graphite, but the authors' of that work considered only a triplet solution, rather than the full unrestricted spin solution. If we restrict our system to zero spin ground state only ($S=0$), then the total energy is 35.5 meV higher than the magnetic configuration. Figure Fig. 1.1(a) shows clearly that the spin-polarized density occupies p orbitals of the adatom. The magnetic properties of the C adatom on graphene can be explained via a simple counting argument. Both the two bonded atoms on the surface, as well as the adatom, present a different hybridization: the surface atoms attached to the adatom have a sp^2 - sp^3 hybridization while the adatom stays sp^2 like, as seen in the model of Fig. 1.1(b). Concerning the adatom, the counting of the four carbon electrons is as follows: two electrons participate in the covalent bond with the graphene carbons. From the two remaining electrons, one goes to the dangling sp^2 bond, and another is shared between the sp^2 bond and the p_z orbital. This p_z orbital is orthogonal to the surface orbitals due to symmetry and cannot form any bands, remaining localized and therefore spin polarized. The dangling sp^2 bond will also probably be very slightly spin polarized, but this effect is negligibly small and cannot be seen in Fig. 1.1(a). The half electron of the p_z orbital provides the magnetization of around $0.5 \mu_B$.

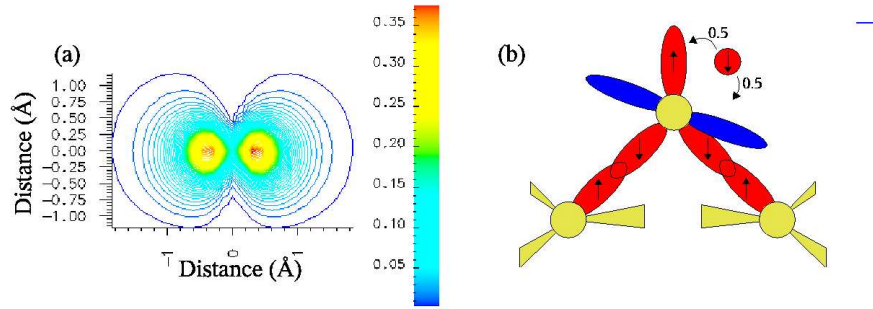


Figure 1.1: (a) The spin density in $e/\text{\AA}^3$ of plane normal to the surface through the center of the adatom when the adatom is at the equilibrium position. The adatom is at $(0,0)$. (b) A schematic diagram of the bond orbitals at the equilibrium position in a plane through the adatom and the two surface carbons. Note that this schematic is a projection, and that the blue p-orbital is orthogonal to the adatom-surface bonds. *Reprinted with permission* [21].

Migration of the adatom

The study of the adatom migration path is crucial in determining the likely state of the defect at a given temperature. If the defect is highly mobile, then it is very likely to diffuse until pinned by interaction with another defect e.g. step-edge, or is annihilated by recombination e.g. adatom meets a vacancy.

The calculated adatom migration path between two equivalent bridge positions is almost a straight line (see Fig. 1.2). The path is calculated using the Nudged Elastic Band method [62]. During the migration between equilibrium positions the magnetic moment disappears because the adatom's hybridization changes from sp^2 to sp -like (only one bond attached to the surface) leaving one dangling bond, and the p_x and p_y orbitals free. The p-orbitals then interact with themselves, creating π -orbitals which interact with the remaining sp -orbital. The result is much more delocalized density and the magnetism is destroyed. The migration energy barrier is 0.47 eV (Fig. 1.3) (0.1 eV within the finite cluster LDA approximation [60]). These facts mean that the adatom is highly mobile on the plane at room temperature and the experimental observation will likely be very difficult without pinning by another defect (see for example Ref. [63]). A possible way to overcome this problem is to use a structure which has finite curvature, for example nanotubes (see subsection 1.3.3). The diffusion through the layers has an energy barrier of 2.3 eV [29] making in-plane motion of the adatom favorable, although as discussed previously we cannot exclude interlayer migration.

1.3.2 Clustering of adatoms

Since we know that adatoms are very mobile on graphene, an obvious question is whether they will form (magnetic) clusters on the surface. The smallest possible cluster is obviously a carbon dimer - the ground state of the dimer on graphene is shown in Fig. 1.4. It has an adsorption energy of 8.7 eV. This system is not magnetic since the the dangling sp^2 bond of the bridge forming carbon ion

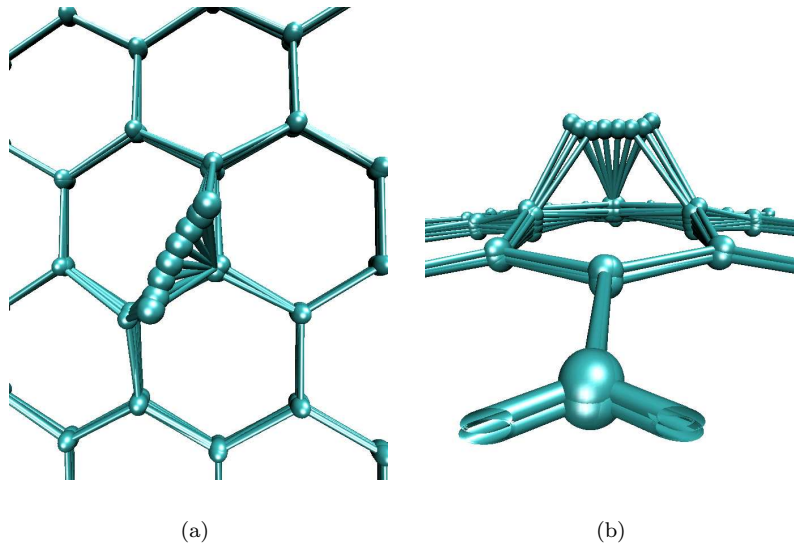


Figure 1.2: Migration path of an adatom on graphene from (a) top and (b) side. The starting point of the path is the equilibrium position and the end point is another equilibrium position. They are both so-called bridge like structures. The middle points of the path where adatom has two bonds is actually a transition point from magnetic to non-magnetic situation. The reason is the change in the hybridisation of the adatom.

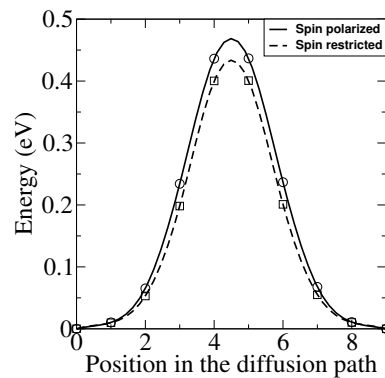


Figure 1.3: Migration energy barrier for a carbon adatom on graphene [21].

forms a bond with the sp -orbital of the upper carbon ion. The p_x -orbital of the carbon ion at the bridge configuration interacts with the p -orbitals of the upper carbon ion becoming a π -orbital as in graphene. As for the adatom alone, the sp -type dangling bond does not have a magnetic moment.

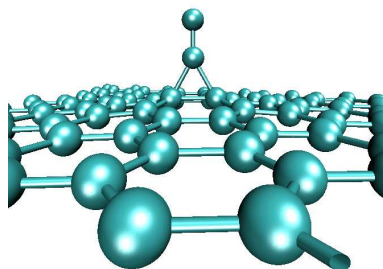


Figure 1.4: The equilibrium structure of a carbon dimer on graphene.

Making a similar calculation with a carbon trimer results in a linear C-C-C equilibrium configuration parallel to the surface plane. Compared to the perfect graphene sheet and three isolated carbon atoms this structure has 12.2 eV lower energy, demonstrating that adatoms will cluster on the surface. In contrast to the dimer, the trimer is magnetic, but with a lower moment than the adatom ($0.2 \mu_B$). Since C-C-C is composed of sp -bonds the conclusion is that the dangling sp -bonds interact first with the p -orbitals preventing the formation of π -orbitals. In general, these results suggest that all clusters with an even number of atoms will be non-magnetic, and all odd will be magnetic - but the moment decays rapidly with the size of the cluster. However, any quantitative conclusions would require an extensive study of cluster growth and include the effects of interlayer interactions.

1.3.3 Adatom on nanotubes

Since the structure and bonding in carbon nanotubes is very similar to that of graphite, it is also interesting to explore whether adatoms are also magnetic on nanotubes. Carbon nanotubes were discovered by Iijima in 1991 [64] and since then the research on carbon systems has increased enormously. Nanotubes are tubular molecules made of pure carbon. They can be considered as graphene sheets rolled into a seamless cylinder - the ends can be either capped or open. Nanotubes are grown as either single walled, or as layered multiwalled tubes. The diameter of a nanotube can vary from a few to a few hundred ångströms while the length scale is from nanometres to centimetres [65].

The electronic structure of a nanotube depends on how the graphene sheet is rolled, i.e. by the so-called chiral vector which connects to crystallographically equivalent points on the underlying graphene sheet. The chiral vector can be expressed in terms of graphene unit vectors, that is designated by a pair of integers (n,m) . Tubes with indices $(n,0)$ are referred to as zigzag and (n,n) as armchair nanotubes. In a simple tight-binding picture, if $n - m$ is a multiple of 3, the tube is metallic, otherwise it is semiconducting. This can be understood in terms of zone folding [66, 67, 68, 69]. However, this description does not take into account the effect of curvature. Due to the curvature of the nanotube the π

and σ orbitals hybridize and thus a small gap opens in zigzag nanotubes. This effect is strongest with nanotubes which have radius less than that of C_{60} [65].

In order to try to sample as wide as possible a family of nanotubes, here we will discuss adatom properties on nanotubes with extreme chiralities i.e. on zigzag and armchair tubes of different radii. The general ground state of an adatom on nanotubes is in a bridge-like structure as in graphite, but the bonds forming the bridge can be either parallel or perpendicular to the tube axis. Figures 1.5 and 1.6 show the equilibrium positions of an adatom on zigzag and armchair nanotubes. The parallel position is shown in Fig. 1.5(a) for a zigzag nanotube and 1.6(a) for an armchair nanotube (the angle between translational axis is less than 45°). The parallel position is a metastable position as can be seen in Table 1.1 [23]. The perpendicular bridge (or perpendicular position of the bridge) has an angle more than 45° with translational axis of the tube (Figs. 1.5(b) and 1.6(b)) and is the true ground state structure.

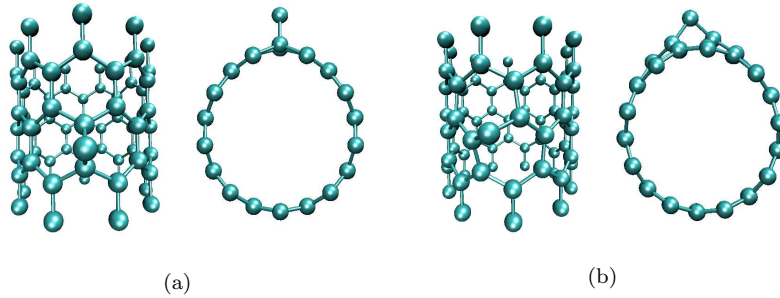


Figure 1.5: Equilibrium positions of an adatom on a (9,0) nanotube in the (a) parallel and (b) perpendicular positions. *Reprinted with permission* [23].

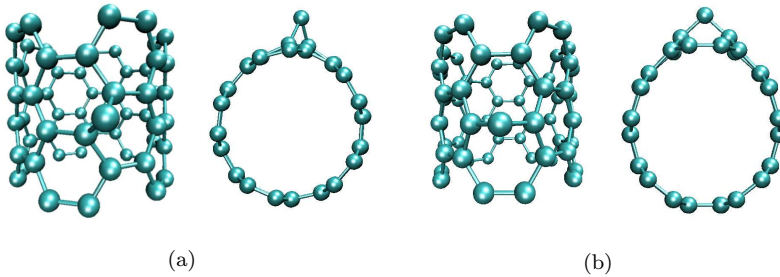


Figure 1.6: Equilibrium positions of an adatom on a (5,5) nanotube in the (a) parallel and (b) perpendicular positions. *Reprinted with permission* [23].

There are three factors to be considered when evaluating the magnetic moment of an adatom: the electronic structure of the tube, the location of the bridge bonds on the tube and the radius of the tube itself. If the nanotube on which the adatom is lying is semiconducting, some of the adatoms charge goes to decreasing the band gap of the tube. If the gap is small enough the tube

Nanotube	Class	Radius (Å)	Adsorption Energy (eV)		Magnetic moment (μ_B)	
			Par.	Perp.	Par.	Perp.
(8,0)	Semiconducting	3.13	2.37	2.89	0.01	0.23
(10,0)	Semiconducting	3.96	2.09	2.57	0.25	0.23
(11,0)	Semiconducting	4.41	2.03	2.49	0.20	0.22
(5,5)	Metallic	3.39	2.33	3.29	0.23	0.44
(9,0)	Semiconducting	3.57	2.35	2.80	0.24	0.35
(6,6)	Metallic	4.07	2.15	2.91	0.27	0.43
(12,0)	Semiconducting	4.97	2.04	2.50	0.32	0.36
Graphene	Metallic	∞	1.40	1.40	0.45	0.45

Table 1.1: Data for the various nanotubes considered in this study. [23].

becomes metallic e.g. (9,0) and (12,0) nanotubes, but for larger gaps they remain semiconducting e.g. (8,0), (10,0) and (11,0). If the unhybridized p-orbital of the adatom is parallel to the translational axis of the tube (as in Fig. 1.6(b)) the situation is very close to graphene, since the curvature of the tube in this direction is the same as graphene's, namely infinite, and nearly the full graphene moment is recovered e.g. (5,5) and (6,6). When an adatom is on a zigzag nanotube at the parallel position (see Fig. 1.5(a)) the p-orbital is perpendicular to the translational axis of the tube. If the tube radius is small enough, as for example in (8,0), the p-orbital interacts with itself around the tube destroying the moment.

Migration of adatoms on nanotubes

Migration of adatoms on nanotubes is important because this issue is directly related to the stability of magnetic defects. Indeed, as we showed above, adatom clustering and annihilation with vacancies gives rise to a decrease or complete disappearance of the magnetic moment.

In order to study migration on nanotubes, we have used two complementary approaches. First we use standard PW-DFT to calculate the adsorption energies for several different nanotubes, and to find the migration path and barrier for one tube. We then use this as a reference to check the accuracy of the computationally cheaper DFT-tight-binding method. Figure 1.7 shows the comparison of adsorption energies, and demonstrates good qualitative agreement - note that the PW-DFT results differ from the DFT-tight-binding (using LDA) by a constant which matches the difference between LDA and GGA in adsorption energies. Figure 1.8 also shows that the migration barrier is also in good agreement, hence we then used DFT-tight-binding to calculate the migration for a large number of tubes. Figure 1.8 shows the barrier as a function of radius for the armchair and zigzag tubes we considered. As expected the barrier decreases with increasing radius, and tends towards the limit of infinite radius i.e. graphene.

1.3.4 Vacancy in graphene

The adatom's partner in the Frenkel pair is the vacancy, hence we apply a similar treatment to study its properties. Initially we consider it in graphene,

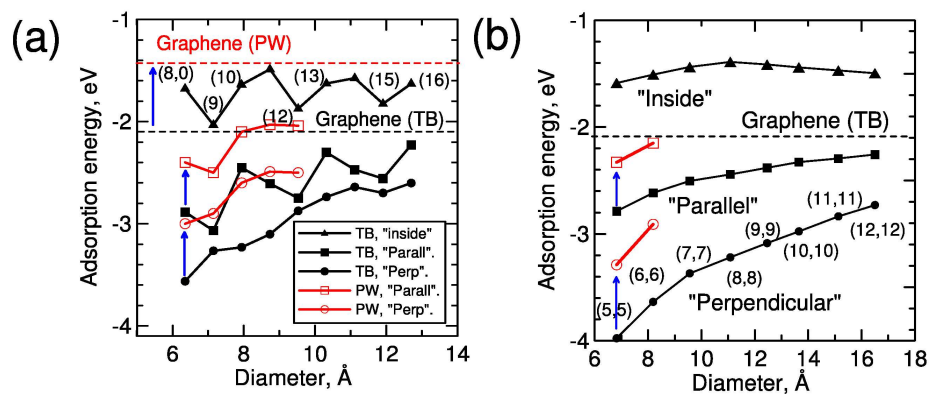


Figure 1.7: Adsorption energies of carbon adatoms on zigzag (a) and armchair (b) single walled nanotubes as a function of nanotube diameters. The arrows visualize the relationships between the corresponding tight-binding and PW results. The numbers stand for the tube chirality indices. *Reprinted with permission* [22].

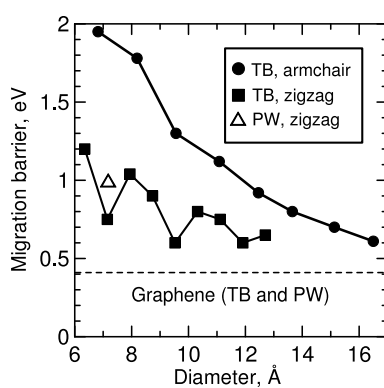


Figure 1.8: Energy barrier for adatom migration on the outer surface on nanotubes as a function of nanotube diameters. Here the graphene migration barrier is the same for the PW and tight-binding calculations. *Reprinted with permission* [22].

and then study the vacancy in a variety of different nanotubes.

The calculated formation energy of a vacancy in graphene is 7.7 eV [24], which is in agreement with previous DFT results of 7.6 eV [70] and 7.4 eV [71]. Atoms 1 and 2 (see Figure 1.9) form a bond creating a pentagon - the distance between atoms 1 and 2 is 2.02 Å compared to the 1.42 Å in ideal graphene. Atom 3 undergoes a Jahn-Teller displacement of about 0.18 Å out of the plane, and the resultant ground state structure is magnetic, with a magnetic moment of $1.04 \mu_B$. This displacement is smaller than the 0.47 Å result of previous spin-restricted calculations [71], but if we set $S=0$ we find a similar displacement of 0.46 Å. This suggests that any predicted inter-planar structures [72, 73] based on the vacancy should be re-examined with the inclusion of spin.

The explanation of the magnetism of the vacancy is as follows: the removal of one carbon ion creates three unsaturated sp^2 -orbitals in the neighboring carbon ions. The formation of the pentagon saturates two of them which leaves one sp^2 -orbital free. This remaining dangling bond contributes the calculated localized magnetic moment as can be seen in the Fig. 1.10.

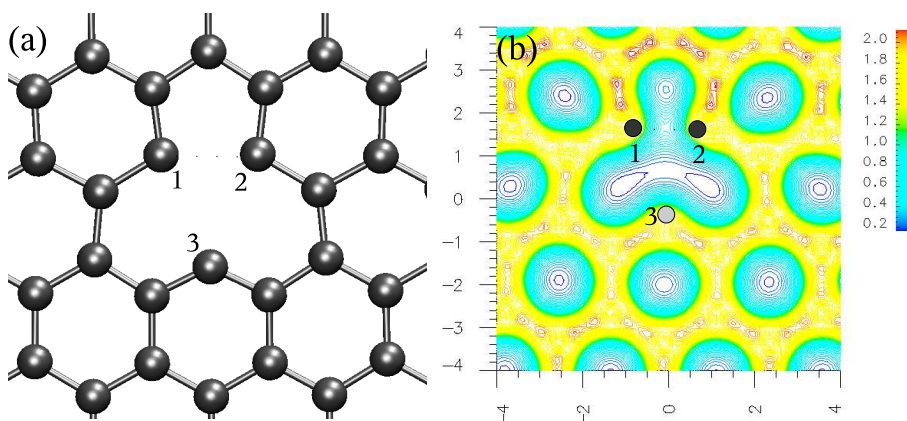


Figure 1.9: (a) Atomic structure of the vacancy in the graphene plane. (b) Charge density of the vacancy in the graphene plane ($e/\text{Å}^3$). [24]

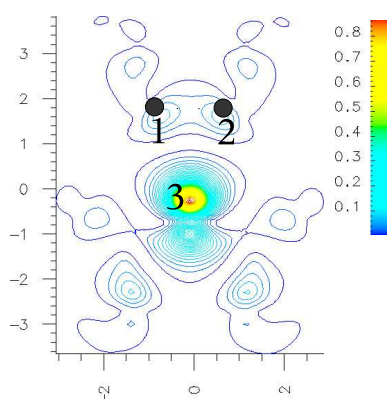


Figure 1.10: Spin density of the vacancy in the graphene plane ($e/\text{Å}^3$). [24]

Migration of a vacancy in graphene

Experimental results have long predicted that the barrier for vacancy migration is quite large, of the order of 3.1 eV [30]. However, theoretical efforts to study this process produce much smaller numbers. GGA-DFT and DFT-TB predict a barrier of 1.4 eV (see Fig. 1.11) in agreement with 1.7 eV in LDA-DFT [71], and other studies [74, 75]. In light of this, it seems likely that the experimentally measured value is actually due to the diffusion of divacancies or larger clusters, but this has yet to be confirmed. Inter-planar migration is much more difficult with migration barriers more than 5 eV for both interstitials and vacancies [30].

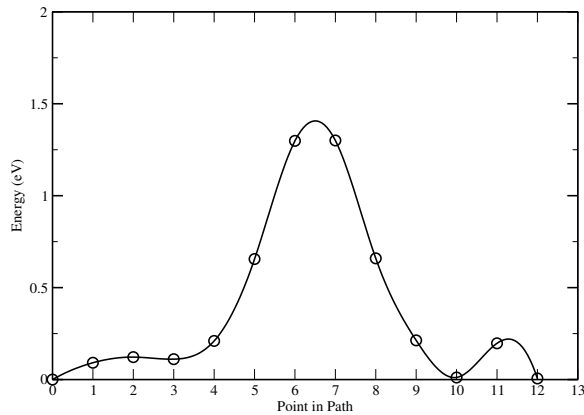


Figure 1.11: The migration energy barrier of a vacancy in graphene.

The migration path calculated using GGA-DFT is shown in Fig. 1.3.4. A switching of bonds occurs between points 10-12 (see Fig. 1.11) which costs 0.2 eV, in agreement with calculations in Ref. [71]. Points #3, #4, #6, #7 and #9 do not carry net magnetic moment. The main difference between points #4 and #5, and on the other hand points #8 and #9, is the bond length of the pentagon bond. In the non-magnetic cases it is 2.00 Å(#4) or 1.98 Å(#9) while in the magnetic case the length of the pentagon bond is 1.87 Å(#5 and #8). The reason for this magnetic moment is the formation of a bond which seems to start with a spin-polarization of sp^2 -orbital.

1.3.5 Vacancy in nanotubes

The description of magnetic properties of a vacancy in nanotubes is a much more difficult task. The properties of a vacancy in a nanotube are due to an interplay the following factors: first, nanotubes are cylinders, not flat planes, and not all carbon atoms are equivalent. Hence, the vacancy may have more than one configuration and all of them need to be checked in order to find the ground state. Secondly, the size of the tube changes when the chirality vector changes. This means that we cannot assume that a general vacancy ground state exists for all tubes regardless of chirality. Thirdly, in nanotubes the electronic structure

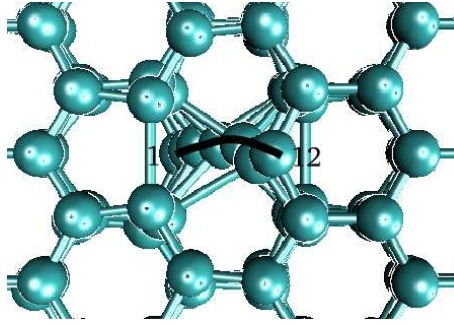


Figure 1.12: Migration path of a vacancy on graphene.

Nanotube	Configuration	E_{for} (eV)	Class	Mag. (μ_B)
(3, 3)	Perp.	4.4	Semi.	0.0
	Par.	5.2	Metal	1.0
(4, 4)	Perp.	5.3	Semi.	0.0
	Par.	6.2	Metal	1.0
(5, 5)	Perp.	5.6	Metal	0.6
	Par.	7.1	Semi.	0.0
(6, 6)	Perp.	5.9	Semi. (Metal ¹)	0.0 (0.4 ¹)
	Par.	7.3	Semi.	0.0

Table 1.2: Properties of the 5-ring armchair SWNTs with vacancies of different configurations. [24]

varies in perfect zigzag nanotubes between semiconducting and metallic, and perfect armchair nanotubes are always metallic. Also, from our calculations on adatoms we know that the electronic structure changes easily when there are defects in the system. In order to study these issues we have considered a large variety of nanotubes, and the results are summarized in Tables 1.2 and 1.3.

The configuration shown in the Figure 1.13(c) has the following properties: each carbon atom is in the sp^2 -hybridization. The atom with a dangling bond has a magnetic moment of $1 \mu_B$ and creates a metallic band. This metallic band is created by the redistribution of the charge within the hexagonal carbon network of the nanotube. In this sense the behaviour is similar to the behaviour of the adatom on the nanotube. However, the magnetic properties of the nanotube with a vacancy depend much more on the curvature of the tube, as does the magnitude of the Jahn-Teller displacement lifting the dangling bond from the surface of the tube.

Figure 1.13(a) shows the ground state of the vacancies for (5,5) and (6,6) nanotubes. The (5,5) nanotube with a vacancy at the perpendicular configuration is magnetic because the Jahn-Teller distortion is large-enough to form the bridge structure (although not sufficient to get $1 \mu_B$). The relaxations of the rest of the tube are small enough so that the overall electronic structure remains metallic. For the (6,6) nanotube, the Jahn-Teller effect is dependent on the linear density of the vacancies along the tube. It is not large enough for a magnetic groundstate if the density is less than 1 vacancy per 4 carbon rings.

Nanotube	Configuration	E_{for} (eV)	Class	Mag. (μ_B)
(5, 0) ¹	Perp.	4.6	Semi.	0.0
	Par.	5.1	Semi.	0.0 ²
	3db	6.0	Semi.	0.0 ²
(6, 0)	Perp.	5.0	Metal	0.3
	Par.	5.8	Metal	0.9
(7, 0)	Perp.	5.2	Semi.	0.0
	Par.	6.3	Metal	0.8
(8, 0)	Perp.	5.3	Semi.	0.0
	Par.	6.5	Metal	0.8
(9, 0)	Perp.	5.4	Semi.	0.0
	Par.	6.4	Metal	1.0
(10, 0)	Perp.	5.5	Semi.	0.0
	Par.	6.7	Metal	0.9
	3db	7.4	Metal	1.9

Table 1.3: Properties of 6-ring zigzag SWNTs with vacancies of different configurations. [24]

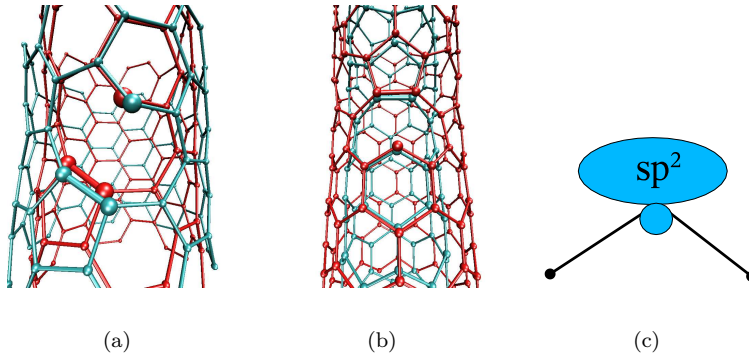


Figure 1.13: The ground state of vacancies in zigzag and armchair nanotubes: (a) (5,5) and (6,6) (opaque) armchair nanotubes, and (b) (6,0) (opaque) and (9,0) zigzag nanotubes. (c) Orbital “bridge” configuration which dominates in vacancy structures in nanotubes.

The smaller radii (3,3) and (4,4) armchair nanotubes demonstrate perfectly the bridge configuration, giving a magnetic moment of $1 \mu_B$ in the perpendicular position.

The bridge configuration is also responsible for the magnetism and metallic electronic structure of the parallel vacancy in larger zigzag-tubes such as (7,0), (8,0), (9,0) and (10,0) (see Fig. 1.13(b)). When the vacancy is in the perpendicular configuration these tubes remain semiconductors, as the removal of the ion increases the gap. The ideal (6,0) nanotube is a metal, and no matter where the vacancy is located, it remains metallic and has a magnetic moment. (5,0) is a semiconductor due to extensive damage on the networks caused by the vacancy on a small tube, preventing the formation of a metallic band.

The question as to what happens when we have an open ended nanotube was studied in Ref. [13]. If the other end of a nanotube is capped with a fullerene the authors found that the edge atoms have a magnetic moment $1.25 \mu_B$ per dangling bond. If a nanotube has both edges open, the spins of the dangling bonds are antiferromagnetically ordered. If the dangling bonds at one edge are saturated with hydrogen, the spins in the open edge contribute most of the total magnetic moment ($1 \mu_B$ per atom). In the (8,0) nanotube the authors found a small polarization of p-orbitals at carbons attached to the hydrogen atoms at the edge. The magnetic state generated by vacancies, zigzag edges at nanotube ends and defective fullerenes are very similar, and point very clearly to the flatband mechanism of magnetism already studied in Refs. [10, 76].

1.4 Magnetism stimulated by non-magnetic impurities

In addition to creating intrinsic defects in carbon materials, ion irradiation may also lead to doping of the sample by the impinging ions. Specifically, the irradiation of graphite by protons has been shown experimentally to induce a significant magnetic signal [19] (see also chapter [Esquinazi]). Since similar irradiation by helium ions produce a much weaker signal, it cannot be simply explained by the generation of vacancies and adatoms. Hence, here we consider the properties of hydrogen and helium in graphite via DFT-GGA simulations, and examine whether they play role in the observed magnetism.

The adsorption energy of H on perfect graphene is 0.87 eV (0.71 eV in Ref. [77], 0.76 eV in Ref. [78], 0.76 eV in Ref. [79] and 0.67 eV in Ref. [80]) and the adsorption position is above another carbon ion. This configuration has no magnetic moment unless the density of hydrogen on the surface is very high, i.e. approaching a few percent [79]. In any case, above a graphene sheet the hydrogen is quite mobile (barrier 1.30 eV for an isolated H on graphene, but reducing to 0.48 eV near other H atoms [78]) and does not form a dimer easily since the barrier for recombination is 2.82 eV [78]. Hence it is highly probable that hydrogen migrates on the plane until it is pinned by another defect.

If the hydrogen encounters an empty vacancy, then it saturates the dangling bond and is pinned at a height of 1.25 \AA above the plane, with an adsorption energy of 4.36 eV. This configuration is non-magnetic. This result contrasts with studies of the effect of a hydrogen on a vacancy-like defect in fullerenes [17], where a magnetic moment of $3.0 \mu_B$ per C_{60} -cage was observed. However, the

local structure in the fullerenes is different, and the under-coordinated carbons cannot saturate bonds with each other due to the increased strain in the system. Hence, hydrogen saturates only one dangling bond and the local moment is provided by the other two sites. A similar configuration can be considered in graphene, where hydrogen adsorbs directly into the vacancy, in-plane with the graphene sheet. The hydrogen atom saturates the dangling bond, but also forces the carbon atoms forming the base of pentagon in the vacancy to move away from each other, significantly weakening the bond between them. The resulting magnetic moment is $2.3\mu_B$, and the spin density shows that this is mainly due to two new dangling bonds on the separated carbons. However, this configuration is metastable on a single graphene sheet, with an energy about 1.3 eV higher than the previous structure, and also a very small barrier between the two states. It is possible that the van der Waals interaction from other layers in graphite may stabilize this structure, or at least increase the barrier, but other configurations seem more likely.

Two stable magnetic configurations involving hydrogen do exist in graphite. Firstly, if an hydrogen atom encounters a vacancy which has already been saturated by hydrogen, it will bond to the other side of the vacancy (see Fig. 1.14(a)) with an adsorption energy of 3.2 eV, at a distance of 0.76 Å below the plane - the original H moves to 0.89 Å above the plane. This configuration has a magnetic moment of $1.2\mu_B$ localized on the dangling sp^2 -bond (see Fig. 1.14(b)). Addition of a third hydrogen completes the decoration of the vacancy edges, saturates the remaining dangling bond and thus destroys the magnetism of the vacancy. Adsorption energy to a system already occupied by two hydrogens is 4.0 eV.

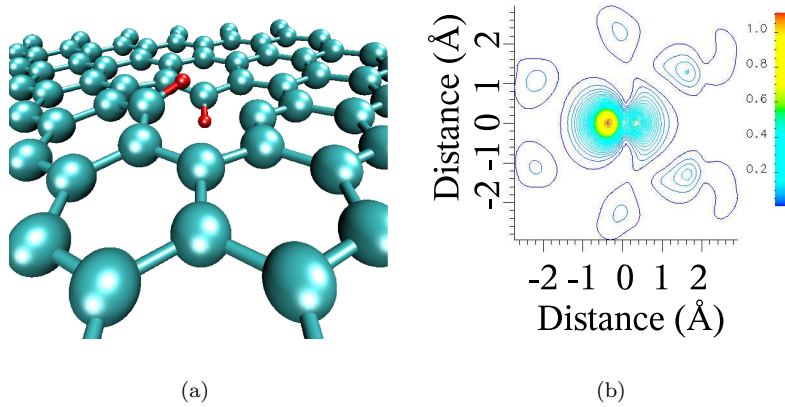


Figure 1.14: (a) Structure and (b) spin density ($\mu_B/\text{Å}^2$) of a vacancy surrounded by two hydrogens.

Secondly, if an hydrogen atom encounters a carbon adatom, they will pin each other (see Fig. 1.15(a)). The C-H bond is tilted due to interaction with the second graphene layer, and H is 2.1 Å above the plane. The adsorption energy of this complex is 3.8 eV. The resulting C-H group has a magnetic moment of $0.9\mu_B$ (see Fig. 1.15(b)).

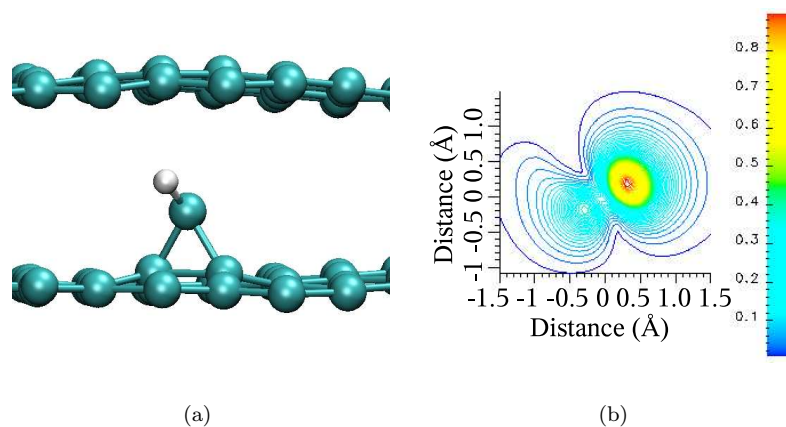


Figure 1.15: (a) Structure and (b) spin density ($\mu_B/\text{\AA}^2$) of a CH group adsorbed between two layers of graphene.

The results for helium irradiation can be similarly understood by calculating the adsorption of He on graphite. DFT predicts that helium has a ground-state adsorption well above graphene sheet, and the interaction between graphite and helium is very weak. This state is non-magnetic. In principle, He will disrupt the magnetism of a vacancy, but the energetic cost to introduce He to a vacancy is very high and it is clear that its main role is in generating defects. Since only a very small magnetic signal is observed in experiments [19], it is reasonable to assume that nearly all vacancies are annihilated by recombination with mobile adatoms.

If we assume that every hydrogen atom introduced by proton irradiation eventually will saturate a carbon dangling bond, then we can predict a rough estimate of the measurable magnetic signal. Two hydrogen atoms at a vacancy result in a moment of $1.2 \mu_B$, and an adatom-hydrogen group provides a moment of $0.9 \mu_B$ from the C-H itself, and $1.0 \mu_B$ from the uncompensated vacancy. Hence, we can consider each hydrogen as providing an average moment of $1.25 \mu_B$. For an experimental dose of $3 \mu\text{C}$ (cf. Fig. 2 in Ref. [19]) of protons we get a signal of $0.2 \mu\text{emu}$ which is in an agreement with the experimental signal $0.3 \pm 0.2 \mu\text{emu}$ and with higher dose of $10 \mu\text{C}$ the predicted signal is $0.8 \mu\text{emu}$ in agreement with $1 \mu\text{emu}$. Obviously, it is very difficult to specify exactly the ratio of different defects that would actually be present in the irradiated material, but the agreement with the experimental magnetic signal strongly suggests that the H-vacancy complex plays a dominant role.

Demonstration of magnetic ordering of the H-vacancy complexes due to the defect-defect interactions from the DFT calculations is beyond the capability of the methods used. However, for adsorbed hydrogen, there are experimental results which indicate that the coupling on graphite can be very long-ranged, even up to 25 lattice constants [81].

Thus, hydrogen contributes to the development of the macroscopic magnetic state in several different ways. Firstly, some defect configurations formed by vacancies and H atoms are magnetic. Secondly, hydrogen prevents complete

recombination of Frenkel pairs, which should increase the number of intrinsic defects (without H). And finally, H atoms appear to favour the development of the long-range magnetic order.

In addition to H-induced magnetism, other non-magnetic elements can give rise to magnetism in graphitic, i.e. π -electron systems. For example, substitutional doping with N/B atoms has been long predicted to give rise to magnetic effects in the sp^2 systems [82]. It is also interesting to note that our calculations predict that doping of nanotubes with nitrogen greatly increases the propensity of point defects to form a magnetic ground state, due to the effective introduction of an extra electron to the system [83]. Nitrogen substituted into the lattice of graphene and nanotubes also acts as a trap for mobile adatoms, providing another avenue for producing localized spin polarized states.

1.5 Conclusions and outlook

In the Introduction to the Chapter, we formulated the most important problems to be attacked before the complete understanding of the magnetism in carbon system is achieved. We further summarized the theoretical findings which shed light on two of the problems. Specifically, we addressed the local bonding geometry which gives rise to local magnetic moments and the role of non-magnetic impurity atoms like hydrogen. Our results, along with those obtained by other authors, provide strong evidence for defect-mediated mechanism of magnetism in carbon systems, although contributions from other mechanisms cannot be excluded in some systems, e.g., carbon foams.

As for graphite, our simulations indicate that adatoms and vacancies on a graphene sheet provide a localized magnetic moment - about $0.5 \mu_B$ and $1.0 \mu_B$ respectively. For a Frenkel pair concentration of 2 ppm, this would result in a magnetic signal of about 10^{-3} emu/g, the experimental value reported in [6]. Correspondingly, the defect concentration should be increased by a factor of about five hundred to explain the recently reported magnetic signal of 0.58 emu/g [4]. It is worth mentioning that the authors of Ref. [4], who explained magnetism in terms of defects (without specifying the defect types), estimated a similar concentration. In general such relatively high defect densities can be reached by irradiation [30] or chemical treatment [4].

In practice, however, the high mobility of adatoms on graphene at room temperature would suggest that many of them recombine with vacancies or cluster together, destroying their magnetism. Despite the indications that a barrier to vacancy-interstitial pair recombination exists [63], efficient recombination seems to be confirmed by He-irradiation experiments [19]. We know a large amount of point defects were produced by He ions, yet the magnetic signal was small. Moreover, as we pointed out in the introduction, not all defects with a localized magnetic moment will participate in the formation of the ferromagnetic state, and may result just in paramagnetism. These factors suggest that, at least for graphite, intrinsic carbon defects, such as interstitials and vacancies cannot explain the observed magnetism.

The demonstration of induced ferromagnetism by proton irradiation on graphite [19] indicates a promising direction for creating magnetic carbon system in a controllable way. Simulations show that this is due to a combination a hydrogen trapping at vacancies and pinning of mobile adatoms, producing magnetic C-H

complexes and uncompensated vacancies. Hydrogen contributes to the development of the macroscopic magnetic state in several different ways. In addition to magnetic defect configurations formed by vacancies and H atoms, hydrogen prevents complete recombination of Frenkel pairs, which should increase the number of defects without H. Also, H atoms appear to favour the development of long-range magnetic order [81].

For nanotubes the situation is even more complicated than in graphite. The surface curvature provides an increase in the adatom migration barrier and, hence, should increase the probability of stable magnetic defects, but the dependence of nanotube electronic structure on chirality affects the picture. Only for adatoms on armchair nanotubes is the defect picture similar to graphene, and both adatoms and vacancies on many other nanotubes are non-magnetic. Some configurations provide a delocalized magnetic band, so, in principle, these would avoid issues of paramagnetism - but controlled production of nanotubes with a specific chirality is currently not possible.

As for fullerene systems, the differences in atomic structures from graphite and nanotubes mean that point defect like vacancies [11] and/or defected fullerenes (open-cage structures) [13, 17] can possibly exist even at room and higher temperatures, and the concentration of defected fullerenes can be high enough to provide agreement with the experimental results. Hydrogen may be also important for the development of the ferromagnetic state in polymerized fullerenes [17].

To sum up, we believe that magnetism in various carbon systems may be associated with defects. Hydrogen may also be very important as it suppresses defect annealing and annihilation. However, the types of defects resulting in the magnetic state in a particular material and the role of hydrogen and other non-magnetic impurities should be studied in more detail, for example, by irradiating the samples with energetic particles. To some extent, this has been already done in experimental work discussed previously [19]. However, systematic studies on irradiation of all-carbon systems with particles of different types and energies should give much more insight into the origin of magnetism. The irradiation temperature is also very important. For example, if carbon interstitials and vacancies can indeed contribute to magnetism then irradiation with electrons or inert gas ions at low (liquid helium or nitrogen) temperature followed by *in situ* magnetic measurements should detect a magnetic signal from the samples. By changing the temperature and thus controlling annealing of defects in the system one can, in principle, correlate magnetism to specific defect types, as different defects become mobile at different temperatures. Irradiation can also be used to introduce non-magnetic impurities like H or N/B atoms into the system, and thus aid in understanding the role of these impurities in the formation of the magnetic state.

Bibliography

- [1] Y. Kopelevich, P. Esquinazi, J.H.S. Torres, and S. Moehlecke. *J. Low Temp. Phys.*, 119:691, 2000.
- [2] T.L. Makarova, B. Sundqvist, R. Hhne, P. Esquinazi, Y. Kopelevich, P. Scharff, V.A. Davydov, L.S. Kashevarova, and A.V. Rakhmanina. *Nature*, 413:716, 2001.
- [3] A. V. Rode, E. G. Gamaly, A. G. Christy, J. G. Fitz Gerald, S. T. Hyde, R. G. Elliman, B. Luther-Davies, A. I. Veinger, J. Androulakis, and J. Giapintzakis. *Phys. Rev. B*, 70:054407, 2004.
- [4] A. W. Mombrú, H. Pardo, R. Faccio, O. F. de Lima, E. R. Leite, G. Zanelatto, A. J. C. Lanfredi, C. A. Cardoso, and F. M. Araújo-Moreira. *Phys. Rev. B*, 71:100404, 2005.
- [5] T. L. Makarova. Magnetism of carbon-based materials. In A. Narlikar, editor, *Studies of High-Temperature Superconductivity*, volume 45, chapter 7, page 107. Nova Science, Huntington, New York, 2003.
- [6] P. Esquinazi, A. Setzer, R. Höhne, C. Semmelhack, Y. Kopelevich, D. Spemann, T. Butz, B. Kohlstrunk, and M. Lösche. *Phys. Rev. B*, 66:024429, 2002.
- [7] T. L. Makarova. *J. Magnetism and Magnetic materials*, xxx:xxx, 2004.
- [8] M. Fujita, K. Wakabayashi, K. Nakada, and K. Kusakabe. *J. Phys. Soc. Jpn.*, 65:1920, 1996.
- [9] Y. Shibayama, H. Sato, T. Enoki, and M. Endo. *Phys. Rev. Lett.*, 84:1744, 2000.
- [10] K. Nakada, M. Fujita, G. Dresselhaus, and M. S. Dresselhaus. *Phys. Rev. B*, 54:17954, 1996.
- [11] A. N. Andriotis, M. Menon, R. M. Sheetz, and L. Chernozatonskii. *Phys. Rev. Lett.*, 90:026801, 2003.
- [12] K. Kusakabe and M. Maruyama. *Phys. Rev. B*, 67:092406, 2003.
- [13] Y.-H. Kim, J. Choi, K. J. Chang, and D. Tománek. *Phys. Rev. B*, 68:125420, 2003.
- [14] D. V. Khveshchenko. *Phys. Rev. Lett.*, 87:206401, 2001.

- [15] D. V. Khveshchenko. *Phys. Rev. Lett.*, 87:246802, 2001.
- [16] N. Park, M. Yoon, S. Berber, J. Ihm, E. Osawa, and D. Tománek. *Phys. Rev. Lett.*, 91:237204, 2003.
- [17] J. A. Chan, B. Montanari, J. D. Gale, S. M. Bennington, J. W. Taylor, and N. M. Harrison. *Phys. Rev. B*, 70:041403, 2004.
- [18] S. Okada and A. Oshiyama. *J. Phys. Soc. Jpn*, 72:1510–1515, 2003.
- [19] P. Esquinazi, D. Spemann, R. Hhne, A. Setzer, and T. Butz. *Phys. Rev. Lett.*, 91:227201, 2003.
- [20] K. h. Han, D. Spemann, P. Esquinazi, R. Höhne, V. Riede, and T. Butz. *Adv. Mater.*, 15:1719, 2003.
- [21] P. O. Lehtinen, A.S. Foster, A. Ayuela, A. Krasheninnikov, K. Nordlund, and R. M. Nieminen. *Phys. Rev. Lett.*, 91:017202, 2003.
- [22] A. V. Krasheninnikov, K. Nordlund, P.O. Lehtinen, A.S. Foster, A. Ayuela, and R.M. Nieminen. *Phys. Rev. B*, 69:073402, 2004.
- [23] P. O. Lehtinen, A. S. Foster, A. Ayuela, T. T. Vehviläinen, and R. M. Nieminen. *Phys. Rev. B*, 69:155422, 2004.
- [24] Yuchen Ma, P. O. Lehtinen, A. S. Foster, and R. M. Nieminen. *N. J. Phys.*, 6:68, 2004.
- [25] N. W. Ashcroft and N. D. Mermin. *Solid State Physics*. Thomson Learning, 1976.
- [26] A. J. Stone and D. J. Wales. *Chem.Phys.Lett.*, 128:501–503, 1986.
- [27] C. P. Ewels, M. I. Heggie, and P. R. Briddon. *Chem. Phys. Lett.*, 351:178–182, 2002.
- [28] J. F. Ziegler, J. P. Biersack, and U. Littmark. *The Stopping and Range of Ions in Matter*. Pergamon, New York, 1985.
- [29] F. Banhart. *Rep. Prog. Phys.*, 62:1181–1221, 1999.
- [30] P. A. Thrower and R. M. Mayer. *Phys. Stat. Sol. (a)*, 47:11, 1978.
- [31] A. V. Krasheninnikov and K. Nordlund. *Nucl. Instr. and Meth. in Phys. Res. B*, 216:355–366, 2004.
- [32] P. Partyka, Y. Zhong, K. Nordlund, R. S. Averback, I. K. Robinson, and P. Ehrhart. *Phys. Rev. B*, 64:235207, 2002.
- [33] T. Diaz de la Rubia, R. S. Averback, R. Benedek, and W. E. King. *Phys. Rev. Lett.*, 59:1930–1933, 1987. See also erratum: *Phys. Rev. Lett.* 60 (1988) 76.
- [34] P. M. Ajayan, V. Ravikumar, and J.-C. Charlier. *Phys. Rev. Lett.*, 81:1437–1440, 1998.

- [35] A. V. Krasheninnikov, K. Nordlund, and J. Keinonen. *Phys. Rev. B*, 65:165423, 2002.
- [36] G.Kresse and J. Furthmüller. *Comp. Mat. Sci.*, 6:15, 1996.
- [37] G.Kresse and J. Furthmüller. *Phys. Rev. B*, 54:11169, 1996.
- [38] J. P. Perdew, J. A. Chevary, S. H. Vosko, K. A. Jackson, M. R. Pederson, D. J. Singh, and C. Fiolhais. *Phys. Rev. B*, 46:6671, 1992.
- [39] G. Makov and M. C. Payne. *Phys. Rev. B*, 51:4014, 1995.
- [40] L. N. Kantorovich. *Phys. Rev. B*, 60:15476, 1999.
- [41] J. Laegsgaard and K. Stokbro. *Phys. Rev. Lett.*, 86:2834, 2001.
- [42] J. L. Gavartin, P. V. Sushko, and A. L. Shluger. *Phys. Rev. B*, 67:035108, 2003.
- [43] G. Pacchioni, F. Frigoli, D. Ricci, and J. A. Weil. *Phys. Rev. B*, 63:054102, 2001.
- [44] L. Hedin. *Phys. Rev. A*, 139:796, 1965.
- [45] D. Cepperley, G. Chester, and M. Kalos. *Phys. Rev. B*, 16:3081, 1971.
- [46] M. Petersilka, U. J. Grossman, and E. K. U. Gross. *Phys. Rev. Lett.*, 76:1212, 1996.
- [47] A. D. Becke. *J. Chem. Phys.*, 98:5648, 1993.
- [48] J. Muscat, A. Wander, and N. M. Harrison. *Chem. Phys. Lett.*, 342:397, 2001.
- [49] C. Lee, W. Yang, and R. G. Parr. *Phys. Rev. B*, 37:785, 1988.
- [50] H. Rydberg, M. Dion, N. Jacobson, E. Schröder, P. Hyldgaard, S. I. Simak, D. C. Langreth, and B. I. Lundqvist. *Phys. Rev. Lett.*, 91:126402, 2003.
- [51] D. Vanderbilt. *Phys. Rev. B*, 41:7892, 1990.
- [52] G. Kresse and J. Hafner. *J. Phys.: Condens. Matter*, 6:8245, 1994.
- [53] G. Kresse and D. Joubert. *Phys. Rev. B*, 59:1758, 1999.
- [54] P. E. Blöchl. *Phys. Rev. B*, 50:17953, 1994.
- [55] D. Porezag, T. Frauenheim, T. Köhler, G. Seifert, and R. Kaschner. *Phys. Rev. B*, 51:12947, 1995.
- [56] M. Elstner, D. Porezag, G. Jungnickel, J. Elsner, M. Haugk, T. Frauenheim, S. Suhai, and G. Seifert. *Phys. Rev. B*, 58:7260, 1998.
- [57] T. Frauenheim, G. Seifert, M. Elstner, T. Niehaus, C. Köhler, M. Amkreutz, M. Sternberg, Z. Hajnal, A. Di Carlo, and S. Suhai. *J. Phys.: Condens. Matter*, 14:3015, 2002.

- [58] A. V. Krasheninnikov, K. Nordlund, M. Sirviö, E. Salonen, and J. Keinonen. *Phys. Rev. B*, 63:245405, 2001.
- [59] J. Keinonen, K. Nordlund, and T. Mattila. *Phys. Rev. Lett.*, 77:699, 1996.
- [60] M. Heggie. *Electrochemical Society Proceedings*, 98-8:60, 1997.
- [61] Y. H. Lee, S. G. Kim, and D. Tománek. *Phys. Rev. Lett.*, 78:2393, 1997.
- [62] H. Jónsson, G. Mills, and G. K. Schenter. *Surf. Sci.*, 324:305, 1995.
- [63] A. Hashimoto, K. Suenaga, A. Gloter, K. Urita, and S. Iijima. *Nature*, 420:870, 2004.
- [64] S. Iijima. *Nature*, 354:56, 1991.
- [65] R. Saito, M. Fujita, G. Dresselhaus, and M. S. Dresselhaus. *Physical Properties of Carbon Nanotubes*. Imperial College London Press, London, 1998.
- [66] N. Hamada, S. I. Sawada, and A. Oshiyama. *Phys. Rev. Lett.*, 68:1579, 1992.
- [67] J. W. Mintmire, B. I. Dunlap, and C. T. White. *Phys. Rev. Lett.*, 68:631, 1992.
- [68] M. S. Dresselhaus, G. Dresselhaus, and R. Saito. *Phys. Rev. B*, 45:6234, 1992.
- [69] O. Gülseren, T. Yildirim, and S. Ciraci. *Phys. Rev. B*, 65:153405, 1992.
- [70] E. Kaxiras and K. C. Pandey. *Phys. Rev. Lett.*, 72:1878, 1988.
- [71] A. A. El-Barbary, R. H. Telling, C. P. Ewels, M. I. Heggie, and P. R. Briddon. *Phys. Rev. B*, 68:144107, 2003.
- [72] R. H. Telling, C. P. Ewels, A. A. El-Barbary, and M. I. Heggie. *Nature Materials*, 2:333, 2003.
- [73] C. P. Ewels, R. H. Telling, A. A. El-Barbary, M. I. Heggie, and P. R. Briddon. *Phys. Rev. Lett.*, 91:025505, 2003.
- [74] E. Kaxiras and K. C. Pandey. *Phys. Rev. Lett.*, 61:2693, 1988.
- [75] C. H. Xu, C. Z. Wang, C. T. Chan, and K. M. Ho. *Phys. Rev. B*, 47:9878, 1993.
- [76] S. Okada and A. Oshiyama. *Phys. Rev. Lett.*, 87:146803, 2001.
- [77] Y. Ferro, F. Marrinelli, and A. Allouche. *J. Chem. Phys.*, 116:8124, 2002.
- [78] Y. Ferro, F. Marrinelli, and A. Allouche. *J. Chem. Phys.*, 368:609, 2003.
- [79] E. J. Duplock, M. Scheffler, and P. J. D. Lindan. *Phys. Rev. Lett.*, 92:225502, 2004.
- [80] X. Sha and B. Jackson. *Surf. Sci.*, 496:318, 2002.

- [81] P. Ruffieux, O. Gröning, P. Schwaller, L. Schlapbach, and P. Gröning. *Phys. Rev. Lett.*, 84:4910, 2000.
- [82] I. Hagiri, N. Takahashi, and K. Takeda. *J. Phys. Chem. A*, 108:2290–2304, 1994.
- [83] Yuchen Ma, A. S. Foster, A. V. Krasheninnikov, and R. M. Nieminen. *J. Phys: Cond. Matter (submitted)*, 2005.
- [84] P. O. Lehtinen, A. S. Foster, Yuchen Ma, A. Krasheninnikov, and R. M. Nieminen, *Phys. Rev. Lett.* 93:187202, 2004.